Talanta 207 (2020) 120290

Contents lists available at ScienceDirect

Talanta

journal homepage: www.elsevier.com/locate/talanta

Ultrasensitive fluorescent detection of HTLV-II DNA based on magnetic nanoparticles and atom transfer radical polymerization signal amplification

Xiaoke Zheng[a], Liying Zhao[a], Dongxiao Wen[a], Xiaolan Wang[a], Huaixia Yang[a], Weisheng Feng[a,*], Jinming Kong[b,**]

[a] Pharmacy College, Henan University of Chinese Medicine, Zhengzhou 450046, PR China
[b] School of Environmental and Biological Engineering, Nanjing University of Science and Technology, Nanjing 210094, PR China

ARTICLE INFO

Keywords:
Fluorescent biosensor
Signal amplification
Atom transfer radical polymerization
Magnetic nanoparticles
HTLV-II DNA

ABSTRACT

Human T-lymphotropic virus type II (HTLV-II) is a crucial retrovirus that is closely associated with a variety of human diseases. Herein, an ultrasensitive fluorescent HTLV-II DNA detection strategy was developed for the first time based on magnetic nanoparticles (MNPs) and atom transfer radical polymerization (ATRP) amplification. In this approach, hairpin DNA probes (pDNA) labelled with 5′ thiol and 3′ azide group terminally were immobilized on amino group modified MNPs surface through sulfo-N-succinimidyl-4-maleimidobutyrate sodium salt (sulfo-GMBS) cross-linkers. In the presence of target DNAs (tDNA), pDNA hybridized with tDNA to form double-stranded DNA, and therefore its azide group was away from the MNPs surface. Subsequently, to initiate ATRP reaction, initiators were introduced into the pDNA by a Cu (I)-catalyzed alkyne-azide cycloaddition (CuAAC). Then, large numbers of 9-anthracenylmethyl methacrylate polymer (pAMMA) were successfully labelled on the MNPs surface, resulting in significant amplification of the fluorescence signal. Under optimized conditions, the fluorescence signal was proportional to the logarithm of the concentration of tDNA over the range from 1 fM to 1 nM, with a detection limit of 0.22 fM. Moreover, this strategy was capable of discriminating mismatched bases and detecting HTLV-II DNA in human serum samples. By virtue of the high sensitivity, selectivity, simplicity and economy, this ultrasensitive biosensor demonstrates great potential for biomedical research and early clinical diagnosis.

1. Introduction

Highly sensitive detection of specific nucleic acid sequences has attracted considerable attention due to its potential application in various fields such as clinical diagnosis [1,2], gene therapies [3,4], and drug screening [5,6]. Human T-lymphotropic virus type II (HTLV-II), being one of human retrovirus, is closely associated with lymphocytic malignancies, neurological disorders, chronic encephalomyelopathy and acquired immune deficiency syndrome [7–9]. Moreover, considering the low abundance of HTLV-II DNA in the human body, short size and high sequence homology among the HTLV family members, the demand for a highly sensitive and selective method to detect HTLV-II DNA and to facilitate the diagnosis and treatment of infectious diseases is increasing [10,11]. Currently, various strategies for target nucleotides detection have been developed based on DNA hybridization, including optical [12], electrochemical [13] and piezoelectric methods [14]. Among these detection approaches, fluorescence method stands out due to their inherent high sensitivity, simple operation, rapid response and noninvasiveness [15,16]. For ultrasensitive fluorescent detection, reasonable design of fluorescent probe is critical. Recently, hairpin DNAs have been used extensively in probe design. Compared to normal DNA probes, hairpin DNA probes have a stem-loop structure as well as good specificity and low background interference [17,18].

Because of the low abundance of HTLV-II DNA in human serum and the difficulty of direct detection, many amplification techniques based on target amplification or signal amplification have been developed to improve the signal output [1]. These include real-time polymerase chain reaction [19], rolling circle amplification [20], gold nanoparticles [21], bio-bar-code [22] and microarray amplification [23]. Although these techniques are sensitive, they inevitably involve complicated preparation, expensive reagents and long operation time, which limit their biomedical application in practical samples [9]. Thus, an effective and economical chemical amplification strategy seems to be an ideal method to improve the sensitivity of DNA detection.

* Corresponding author.
** Corresponding author.
E-mail addresses: fwsh@hactcm.edu.cn (W. Feng), j.kong@njust.edu.cn (J. Kong).

https://doi.org/10.1016/j.talanta.2019.120290
Received 27 May 2019; Received in revised form 6 August 2019; Accepted 20 August 2019
Available online 23 August 2019
0039-9140/

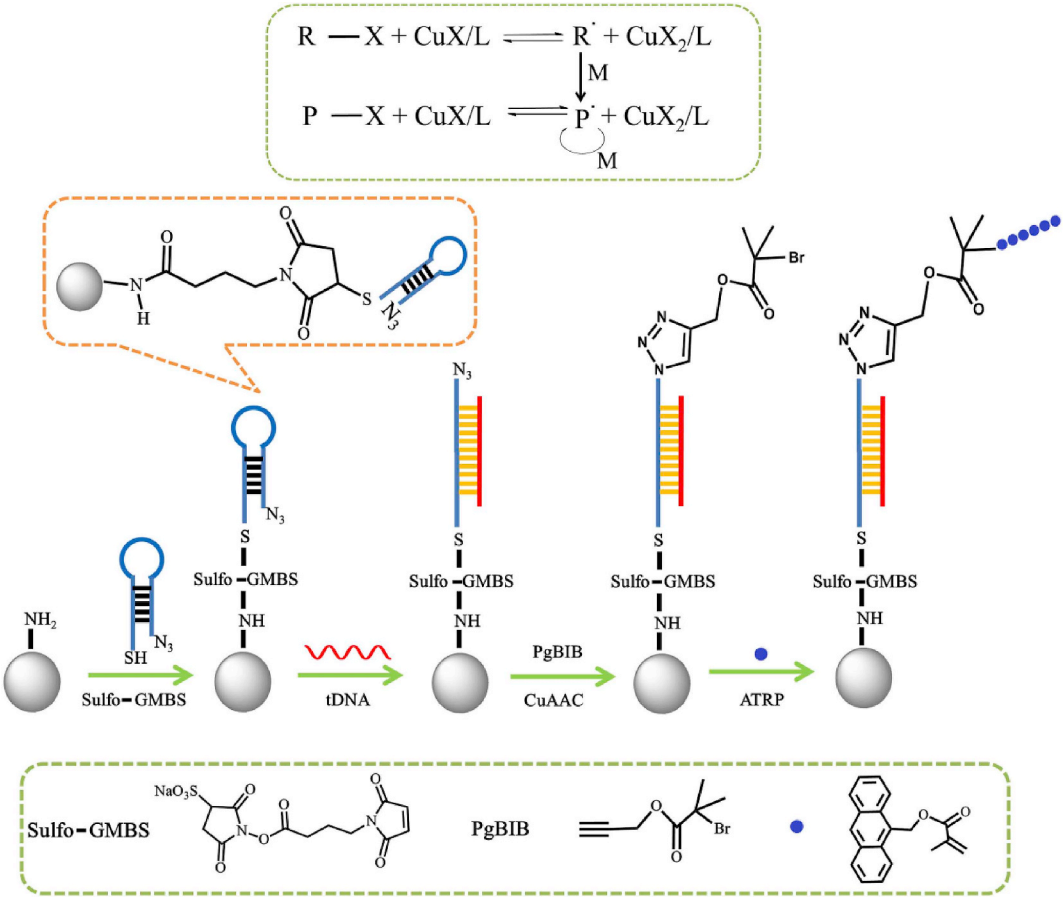

Scheme 1. Schematic illustration of fluorescent biosensor based on ATRP signal amplification.

Controlled radical polymerization (CRP) amplification, a relatively new polymerization amplification technique, involves the growth process of a polymer chain from one initiation event. Especially, it is extremely sensitive to low radical concentrations [24]. CRP-assisted amplification strategies, such as nitroxide-mediated radical polymerization (NMP), reversible addition-fragmentation chain transfer (RAFT) and atom transfer radical polymerization [25,26], have attracted considerable attention because of their high sensitivity, simplicity and low cost. In these polymerization techniques, ATRP is generally recognized as one of the most effective polymerization methods because of its mild reaction conditions, moderate reaction temperature, various monomers and tolerance to oxygen [27,28]. ATRP, which was first reported simultaneously by Matyjaszewski [29] and Sawamoto [30] in 1995, is a strategy for forming C–C bonds that exploits transition metal complex (e.g., Cu^{I}/L, L = ligand) as catalysts for the reaction between alkyl halides and vinyl monomers [31], in which the growth of the polymer chains primarily relies on atom transfer. Briefly, ATRP is a reversible dynamic equilibrium between the active radicals (P •) and the dormant species (alkyl halide initiator: R−X and polymer: P−X, Scheme 1) by redox reaction. In our study, magnetic nanoparticles (MNPs) could modify a large number of probes as carriers. Moreover, the assembly of multiple oligonucleotides on MNPs provided an extremely clean reaction environment for ATRP, which improved the sensitivity and specificity for nucleic acids detection. To the best of our knowledge, the fluorescent detection of HTLV-II DNA on the basis of MNPs and ATRP amplification has not been reported yet.

Herein, we reported the development of an innovative fluorescent biosensor with high sensitivity and specificity for DNA detection based on MNPs and ATRP signal amplification. pDNA, labelled with a thiol and azide group at either terminal, were first immobilized on MNPs through sulfo-GMBS cross-linkers and served as capture probes for the specific recognition of tDNA. After hybridization, initiators of ATRP system were introduced via CuAAC between the azide group of pDNA and the alkynyl of initiators. A large number of monomers with optical property were attached to the pDNA through ATRP reaction. The generated pAMMA can effectively amplify the fluorescence signal. By exploiting the high specificity of hairpin DNA, MNPs and ATRP amplification strategies, the proposed biosensor demonstrated higher sensitivity and selectivity compared to other fluorescent biosensors for DNA detection. Moreover, this signal amplification strategy exhibits good analytical performance in HTLV-II DNA detection and provides a sensitive and economical method for nucleic acids detection.

2. Experimental

2.1. Materials

Magnetic nanoparticles (MNPs, d = 0.2 μm, 10 mg/mL^{-1}) were obtained from PuriMag Biotech, (Xiamen, China), and modified with amino groups on the surface. Tris (2-carboxyethyl) phosphine hydrochloride (TCEP), sulfo-N-succinimidyl-4-maleimidobutyrate sodium salt (sulfo-GMBS), propargyl 2-bromoisobutyrate (PgBIB), tris-(2-dimethylaminoethyl) amine (Me_6TREN) and 9-anthracenylmethyl methacrylate (AMMA) were purchased from Sigma-Aldrich (St. Louis, USA). Ascorbic acid (AA), copper (II) sulfate ($CuSO_4$) and copper (I) bromide (CuBr) were purchased from J&K Scientific Ltd. (Shanghai, China). Normal human serum (NHS) was obtained from Yu Duo Co., Ltd. (Shanghai, China). Ultrapure water (≥18.2 MΩ) obtained using a Millipore filtration system was used in all experiments. All of the other chemicals were of analytical grade and used without further purification.

All oligonucleotides were synthesized and purified using high-

Table 1
Sequences of the oligonucleotides.

Note	Base sequences (5′-3′)
Hairpin DNA probes (pDNA)	SH-ACACGCTCCCCGACCCAATTTCCA CCTTCGCGTGT-N3
Target complementary DNA (tDNA)	CGAAGGTGGAAATTGGGTCGGGGAG
Single base mismatched DNA (SBM)	CGAAGATGGAAATTGGGTCGGGGAG
Three bases mismatched DNA (TBM)	CGCAGGTGGAATTTGGGTAGGGGAG
Non-complementary DNA (cDNA)	GAGGGCCTGCAGGATCATTGGCTTT

performance liquid chromatography from Sangon Biotechnology Co. Ltd. (Shanghai, China). 0.1 M phosphate buffer solution (PBS, pH 7.4) as the reaction solution was prepared for modifying MNPs and fluorescence detection. DNA were dissolved in Tris-EDTA buffer solution (TE, 10 mM Tris-HCl, 1 mM EDTA and pH 8.0) and stored at - 20 °C. pDNA were heated to 95 °C for 2 min, and then slowly cooled to room temperature for 60 min so that it completely folded into a hairpin structure before use. Table 1 listed the base sequences of the oligonucleotides.

2.2. Apparatus

All fluorescent spectra were performed on a FLS 1000 fluorescence spectrophotometer (Edinburgh, UK). Fluorescence images were taken using a confocal laser scanning microscopy (CLSM, Olympus FV 1200, equipped with 10 × and 40 × lenses). Atomic force microscopy (AFM) images were obtained using Dimension Icon (Bruker Nano Inc, USA, scan size = 1.7 μm). High-resolution transmission electron microscopy (HRTEM; JEM-2100, JEOL, 200 kV) was utilized to characterize the morphologies of the different modified MNPs.

2.3. Preparation of MNPs conjugated with pDNA

Prior to use, the thiolated pDNA (1.5 μM) and TCEP solution (1.5 mM) were incubated in the dark for 60 min at 37 °C to reduce the disulfide bonds. MNPs-pDNA conjugates were prepared as reported in the literature [32,33]. First, 20 μL of MNPs (10 mg/mL^{-1}) were washed three times and re-suspended in 180 μL of 0.1 M PBS. Then, 20 μL of 0.1 mM sulfo-GMBS solution (dissolved in PBS) was added and incubated for 30 min at 37 °C. After magnetic separation, excess linkers were removed with 0.1 M PBS. Subsequently, these MNPs were reacted with pDNA (1.5 μM) in a final volume of 200 μL of PBS for 2 h at 37 °C. Afterwards, the MNPs-pDNA were magnetically separated and rinsed with PBS to remove the residual adsorbed oligonucleotides, and then re-suspended in 180 μL of 10 mM TE buffer solution (pH 8.0).

2.4. DNA hybridization and initiator immobilization

20 μL of 10 nM tDNA were incubated with prepared MNPs-pDNA for 105 min at 37 °C. After the specific recognition between pDNA and tDNA, the hairpin structure was opened, resulting in the exposure of the azide group of pDNA on the surface of MNPs-pDNA-tDNA. After magnetic separation, the MNPs were rinsed with 10 mM TE buffer solution (pH 8.0) to remove the unhybridized tDNA, and then re-suspended in 140 μL of 0.1 M PBS. Then, MNPs-pDNA-tDNA were incubated with 20 μL of 10 μM PgBIB, 20 μL of 1 mM $CuSO_4$ and 20 μL of 2 mM AA for 75 min at 37 °C, Subsequently, the generated MNPs-pDNA-tDNA-PgBIB were magnetically separated and rinsed with 70% ethanol and ultrapure water.

2.5. Fluorescent detection of tDNA based ATRP signal amplification

The ATRP mixture was obtained by mixing 20 μL of 10 mM CuBr/Me_6TREN (1:1.2 in molarity dissolved in DMF), 20 μL of 5 mM AMMA (dissolved in acetonitrile), 20 μL of acetonitrile and 140 μL of 0.1 M PBS. The polymerization of AMMA via ATRP was performed by dispersing the as-prepared MNPs (MNPs-pDNA-tDNA-PgBIB) in the freshly prepared mixture for 60 min at 45 °C. After that, the modified MNPs (MNPs-pDNA-tDNA-PgBIB-pAMMA) were separated and moderately rinsed with acetonitrile and ultrapure water. The fluorescence intensity was measured by adding MNPs-pDNA-tDNA-PgBIB-pAMMA in 3 mL of 0.1 M PBS (pH 7.4). Finally, the fluorescence emission of pAMMA was obtained at an excitation of 252 nm. The slit width of excitation and emission was set to 5 nm. The fluorescence intensity at 412 nm was relatively stronger than at 392 nm and 412 nm, thus fluorescence emission at 412 nm was used to evaluate the performance of the proposed assay [34].

3. Results and discussion

3.1. Principle of fluorescent biosensor for HTLV-II DNA detection

In this study, utilizing fluorescent substance pAMMA as the signal reporting unit and hairpin DNA as the capture probe, a novel fluorescent biosensor was fabricated for HTLV-II DNA detection based MNPs and ATRP amplification. The principle of HTLV-II DNA detection is depicted in Scheme 1. First, sulfo-GMBS as heterobifunctional cross-linkers that include both amino and mercapto reactive functionalities were applied to MNPs conjugated with pDNA. MNPs that modified amine group were initially reacted with the succinimide ester of sulfo-GMBS. Then, the maleimido of sulfo-GMBS connected MNPs reacted with pDNA modified with the terminal thiol group. In the presence of tDNA, the complementarity of tDNA with pDNA caused the hairpin structure to open and the azide group to stay away from the MNPs surface. Then, numerous ATRP initiators were attached to the MNPs via CuAAC reaction. Afterwards, large numbers of AMMA were labelled on the MNPs surface to generate long polymeric chains via ATRP reaction, thereby significantly improving detection sensitivity. In the absence of tDNA, few initiators were introduced on the surface of MNPs and the corresponding fluorescence intensity was very low due to the steric hindrance. In ATRP, common polymer grafting techniques can be categorized into grafting-from and grafting-to approaches [35]. When grafting to the surface, a ready-made polymer is covalently attached to the reactive sites of the surface. Comparatively, the grafting-from method is based on surface-initiated polymerization by the successive addition of monomer from the initiating sites on the surface. Although the former is relatively easy to operate, grafted polymer chains can shield reaction sites on the MNPs as random curling conformation of the chains. However, the latter can provide higher grafting density due to lesser steric hindrance of the monomer compared to the polymer chains. Taking into account the introduction of more AMMA tagged MNPs, the grafting-from strategy is indeed the perfect choice to increase fluorescence signal.

3.2. The feasibility of fluorescent biosensor for HTLV-II DNA detection

In order to verify the feasibility of the fluorescent biosensor for tDNA detection, fluorescent assay with different modified MNPs was performed in 0.1 M PBS (pH 7.4). As shown in Fig. 1(A), at the excitation wavelength of 252 nm, MNPs, MNPs-pDNA, MNPs-pDNA-tDNA, and MNPs-pDNA-tDNA-PgBIB were nearly no fluorescence absorption (except for weak background signal). Moreover, only very low

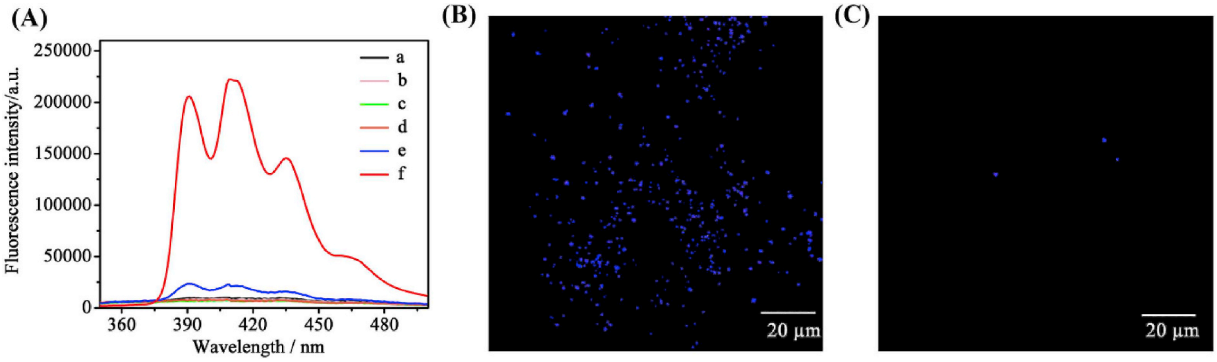

Fig. 1. (A) Fluorescence spectra of (a) MNPs, (b) MNPs-pDNA, (c) MNPs-pDNA-tDNA, (d) MNPs-pDNA-tDNA-PgBIB, (e) MNPs-pDNA-PgBIB-AMMA, (f) MNPs-pDNA-tDNA-PgBIB-AMMA. Fluorescence images of different modified MNPs (B) in the presence and (C) absence of tDNA. (0.1 M PBS, pH 7.4).

fluorescence absorption appeared without tDNA, because pDNA were preserved in a folded form and it was difficult to bind the azide group to the initiators (PgBIB). Remarkably, a strong fluorescent absorption peak appeared when all reagents were added. It suggested that a sufficient number of initiators and AMMA were labelled only when the hairpin structure was unfolded by tDNA. Furthermore, Fig. 1(B) visually indicated that the AMMA was successfully labelled on the MNPs compared to MNPs modified in the absence of tDNA (Fig. 1(C)).

AFM and HRTEM were utilized to characterize the morphologies of different modified MNPs. Fig. 2(A) showed that the surface height of the MNPs immobilized with pDNA was 22.4 nm after CuAAC and ATRP reaction. Fig. 2(B) showed that the MNPs modified with pDNA were incubated sequentially with the hybridization solution (containing tDNA), CuAAC and ATRP reaction solution to obtain a more towering image with a surface height of 34.6 nm. Moreover, the HRTEM images demonstrated that the average size of MNPs was 160 nm in the absence of tDNA (Fig. 2(C)). In contrast, MNPs showed a uniform spherical crystallite with an average diameter of 172 nm in the presence of tDNA (Fig. 2(D)), and the increase in the size of MNPs characterized by TEM was nearly consistent with the change in the height of MNPs characterized by AFM. These experimental results revealed that the fluorescence sensor was successfully fabricated.

3.3. Optimization of experimental conditions

In the fluorescent biosensor construction process, some important experimental parameters required optimization to improve the sensor's efficiency and sensitivity (the other reaction conditions were kept suitable for single condition optimization) [36].

In this study, MNPs could serve as a convenient and efficient tool for separating the substance from a complex biological solution as well as modify a large number of probes as carriers [37]. The concentration of pDNA modified MNPs directly affected the sensitivity and detection range to some extent. Therefore, the effect of MNPs on fluorescence intensity was investigated under a fixed pDNA concentration. As shown in Fig. 3(A), the fluorescence intensity gradually increased with

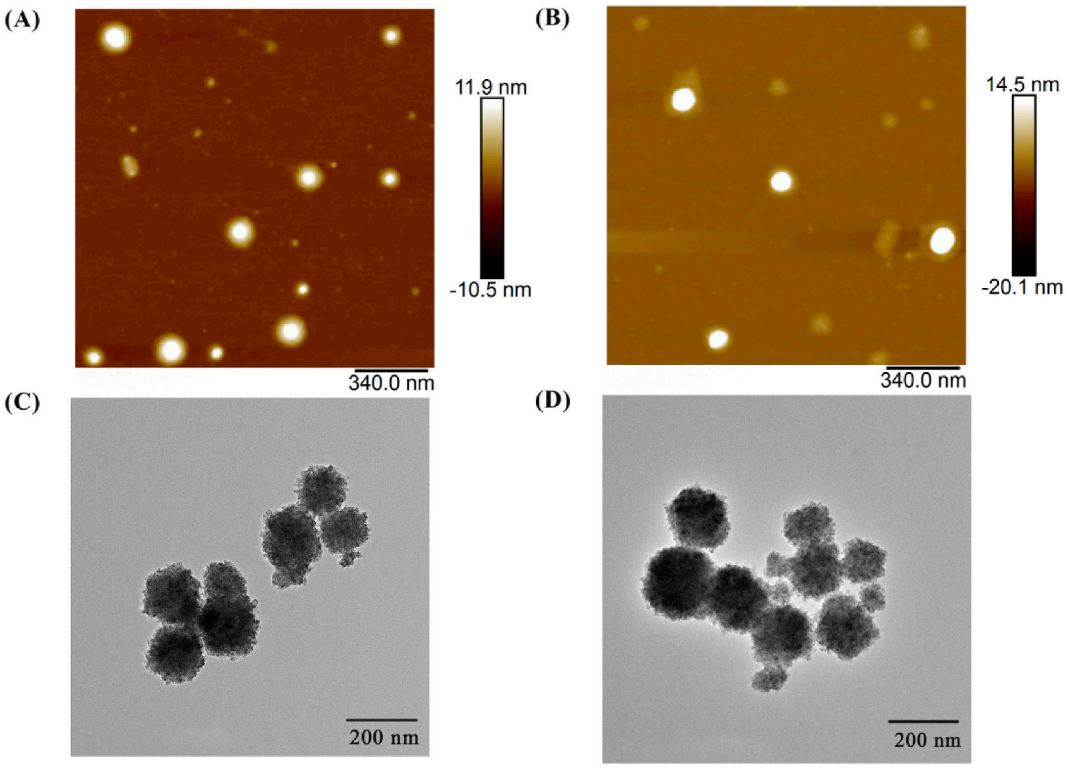

Fig. 2. AFM images of different modified MNPs (A) in the absence and (B) presence of tDNA. HRTEM images of different modified MNPs (C) in the absence and (D) presence of tDNA.

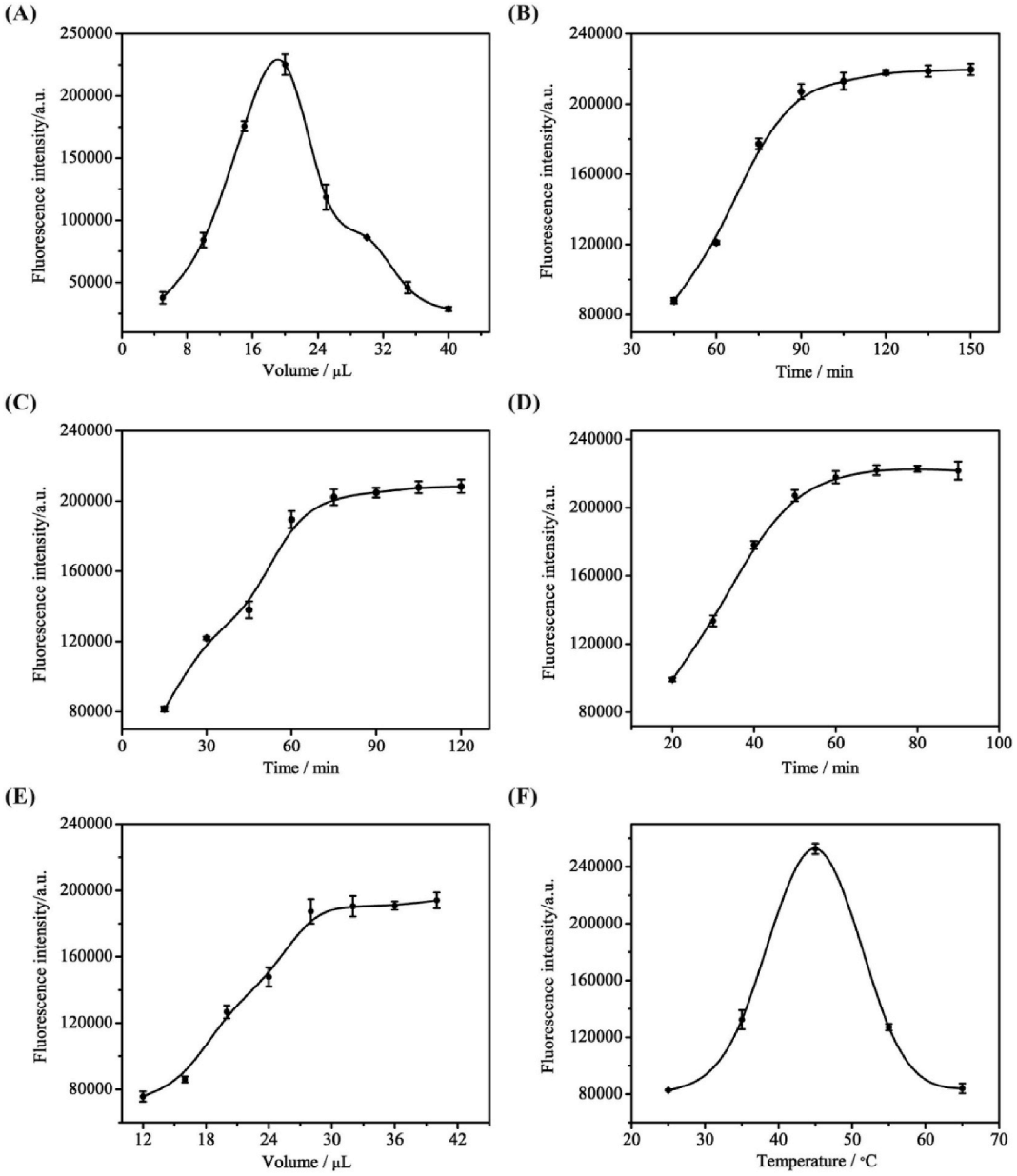

Fig. 3. Influence of different reaction conditions on fluorescent biosensor response. (A) The volume of MNPs (10 mg/mL). (B) DNA hybridization reaction time. (C) CuAAC reaction time. (D) ATRP reaction time. (E) The volume of AMMA. (5 mM) (F) ATRP reaction temperature. Error bars represent the standard deviations of three measurements (excitation wavelength: 252 nm, emission wavelength: 412 nm, 0.1 M PBS (pH 7.4), 1 nM tDNA).

increasing volume of MNPs and reached a maximum at 20 μL which indicated that the concentration of pDNA coated on the MNPs was gradually increased. However, the fluorescence intensity obviously decreased after 20 μL, which may have been caused by the scattering of excess MNPs or quenching of pAMMA by MNPs [38]. Thus, 20 μL of MNPs (10 mg/mL^{-1}) were used for the following experiment.

Furthermore, hybridization reaction time was a significant factor relative to the fluorescent biosensor's sensitivity. Fig. 3(B) showed fluorescence intensity at different hybridization time. A gradual increase of fluorescence intensity can be observed with the hybridization time extending, which reached a plateau at 105 min. Therefore 105 min was selected as the best hybridization reaction time.

For molecular transformation, the CuAAC reaction has emerged as a critical and versatile conjugation tool [39]. In this reaction, the initiators of ATRP reaction were introduced by CuAAC, such that CuAAC reaction time had considerable influence on the fluorescence intensity. As shown in Fig. 3(C), with the increment of the incubation time, more initiators were connected to MNPs. Furthermore, when the incubation time reached 75 min, the fluorescence intensity was essentially unchanged even though the incubation time was extended, which indicated that the connected PgBIB was saturated at 75 min. Therefore, 75 min was chosen as the optimal CuAAC reaction time.

Relevant ATRP reaction conditions affected the polymerization of AMMA, which directly impacted the change in fluorescence intensity. Thus, it was essential to optimize key reaction conditions such as reaction time, AMMA concentration and reaction temperature. It can be seen from Fig. 3(D) that fluorescence intensity significantly increased with the increase of reaction time in 20–50 min. After that, the growth slowed gradually and became saturated after 60 min. As shown in Fig. 3(E), with the increase in AMMA concentration, the fluorescence intensity showed a stable trend after 28 μL (5 mM). Furthermore, reaction temperature was another condition that significantly influenced fluorescence intensity. It can be seen from Fig. 3(F) that the reaction temperature reached a peak at 45 °C, and then fluorescence intensity

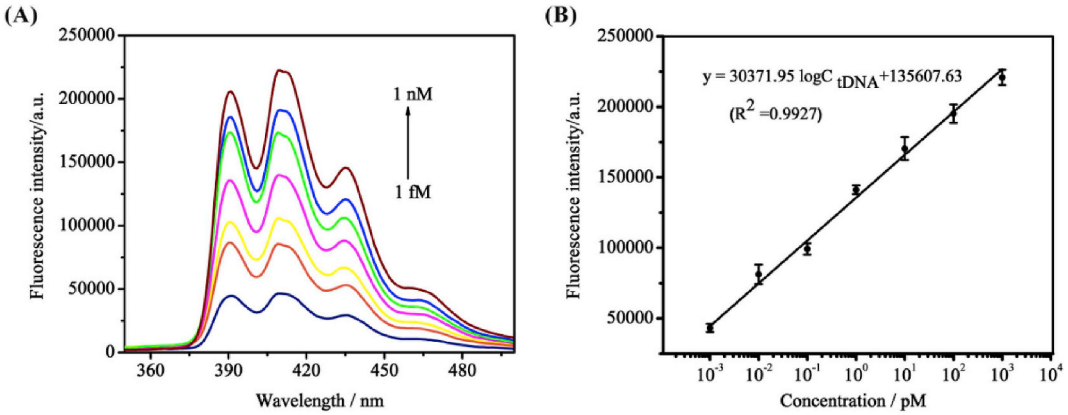

Fig. 4. (A) Fluorescence spectra of different concentrations of tDNA in 0.1 M PBS (pH 7.4). The concentrations of tDNA were 1, 10, 10^2, 10^3, 10^4, 10^5, and 10^6 fM respectively. (B) The linear relationship between fluorescent intensity and logarithm of the tDNA concentration. Error bars represent the standard deviations of three measurements (excitation wavelength: 252 nm, emission wavelength: 412 nm).

significantly decreased with increasing reaction temperature. This is primarily attributable to the slow polymer growth at lower temperatures; conversely the decrease of the fluorescence intensity at high temperatures may be due to the proximity to melting temperature of the complementary strands and poor stability of the polymer fixed on MNPs [40,41]. Accordingly, 60 min, 28 μL (5 mM) of AMMA and 45 °C were selected as the optimal ATRP reaction conditions.

3.4. Analytical performance

The fluorescence intensity of pAMMA was directly related to the initiators modified on the MNPs and amount of initiators were interrelated to tDNA. Based on this, the fluorescence intensity of this biosensor was related to tDNA concentration. Thus, under optimal detection conditions, the response range and detection limit of tDNA were quantitatively evaluated using fluorescence spectroscopy. As shown in Fig. 4, a good linear positive correlation emerged between fluorescence intensity and the logarithm of tDNA concentration in the range of 1 fM to 1 nM. The corresponding regression equation was $F = 30371.95 \log [C_{tDNA}/pM] + 135607.63$ ($R^2 = 0.9927$), and the calculated limit of detection (LOD) was 0.22 fM based on S/N = 3. To further demonstrate the good performance of the fluorescent biosensor, we compared the linear range and LOD characteristics of other sensors reported in the literature (Table 2). The proposed sensor in this study exhibited a wider linear range and lower LOD.

3.5. Selectivity, repeatability, stability of the fluorescent biosensor

Due to the high sequence homology among the HTLV family, the selective detection of HTLV-II DNA has always been a great challenge [9]. To demonstrate the selectivity of the developed method, we measured the fluorescence response to complementary DNA (tDNA), single base mismatched DNA (SBM), three base mismatched DNA (TBM) and non-complementary DNA (cDNA) under the same experimental conditions. The concentration of all DNA was 1 nM. As shown in Fig. 5(A) and Table 2, the fluorescence response of SBM was only 22.9% of tDNA compared to reported biosensor, indicating that this biosensor had high specificity for SBM. The fluorescence response of TBM was almost 80.5% less than that of tDNA, while cDNA was not observably different from background signal. The significant difference in the fluorescence response could be attributed to the efficiency between different oligonucleotides hybridization and pDNA. In addition, the stem of hairpin DNA was not conducive to hybridization between the nucleic acids of the loop and mismatched oligonucleotides [17]. These results indicated that the developed biosensor had high selectivity for complementary and mismatched oligonucleotides.

Five independently prepared probes were used to detect tDNA (1 nM) with a relative standard deviation (RSD) of 2.82%, demonstrating that the prepared fluorescent biosensor had good precision and repeatability. Under the same experimental conditions, five samples were prepared and stored at 4 °C. After 1 month, it was observed that up to 91.5% of the fluorescence intensity was retained; therefore, the fluorescent biosensor demonstrated satisfactory storage stability.

Table 2
Comparison of analytical performance between proposed with reported DNA biosensors.

Method	Linear range	Detection limit	Selectivity[a]	Ref.
Electrochemistry	1 pM to 1 nM	0.62 pM	26%	[42]
Electrochemistry	1 pM to 1 nM	0.171 pM	42.1%	[10]
Electrochemistry	100 nM to 10 fM	10 fM	32%	[43]
Electrochemistry	1 fM to 1 nM	0.47 fM	25.1%	[44]
Fluorescence	0.1 nM to 0.4 μM	5 pM	No	[36]
Fluorescence	0 pM–3 pM	0.58 pM	30%	[45]
Fluorescence	20 fM to 0.1 nM	20 fM	26%	[46]
Fluorescence	1 fM to 1 nM	0.22 fM	22.9%	This work

[a] Percentage response of single base mismatched DNA to complete complementary DNA.

3.6. Analysis of real serum samples

To evaluate the proposed biosensor for real sample analysis, we measured the fluorescence response to tDNA spiked in 5% normal human serum (NHS). As shown in Fig. 5(B), only very low fluorescence absorption was observed in TE buffer solution and 5% NHS (in the absence of tDNA). In the presence of tDNA, a distinct fluorescence signal was detected in tDNA (1 nM) + 5% NHS, similar to the fluorescence intensity detected in only tDNA (1 nM). These results demonstrated that this method had good anti-interference ability in complex serum samples. Furthermore, to calculate the recoveries, three known concentrations of tDNA (0.1 nM, 1 pM, 10 fM) were added into 5% NHS respectively and measured using the designed biosensor. As indicated in Table 3, the recoveries were in the range of 93.02%–98.11% and the RSD was less than 3.5% (n = 3). Therefore, the fabricated biosensor may demonstrate great potentiality for tDNA detection in real serum samples.

4. Conclusions

We developed a promising fluorescent biosensor for ultrasensitive detection of HTLV-II DNA based on MNPs and ATRP signal amplification. The good performance of the fluorescent biosensor is mainly based

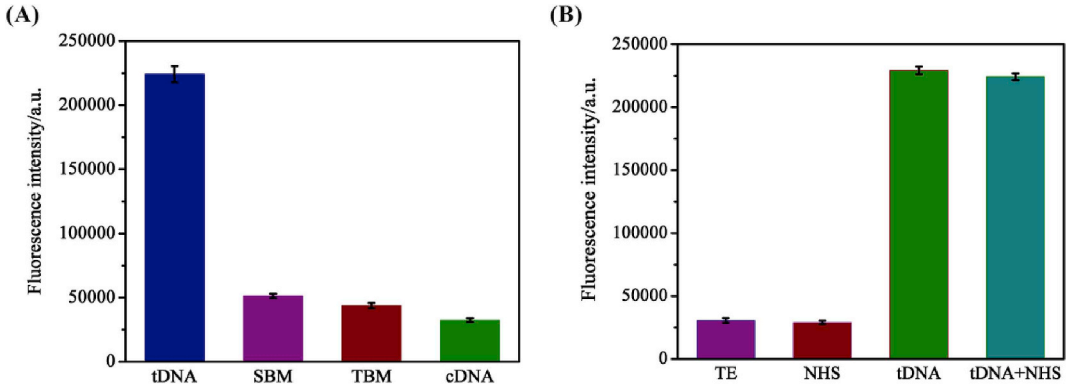

Fig. 5. (A) Selectivity of the fluorescent biosensor toward different oligonucleotide fragments. (B) Detection capability of the fluorescent biosensor in 5% normal human serum (NHS). Error bars represent the standard deviations of three measurements. The concentrations of oligonucleotide fragments were all 1 nM.

Table 3
Determination of tDNA in 5% serum samples (n = 3).

Sample	Added concentration	Found concentration	Recovery	RSD
1	0.1 nM	0.09551 nM	95.51%	2.744%
2	1.0 pM	0.9811 pM	98.11%	1.719%
3	10 fM	9.302 fM	93.02%	3.168%

on controllability and signal amplification of ATRP, efficient separation of MNPs and high specificity of hairpin DNA probes. Under optimal conditions, this method exhibited high sensitivity for HTLV-II DNA detection with a LOD of 0.22 fM. Moreover, it demonstrated good capability to discriminate mismatched bases and detect HTLV-II DNA in human serum samples. Taking advantage of its high sensitivity, selectivity, simplicity and economy, this signal amplification strategy may pave a new approach for HTLV-II DNA detection at trace level and supply an effective assessment for the early diagnosis of other diseases.

CRediT authorship contribution statement

Xiaoke Zheng: Funding acquisition, Methodology, Writing - review & editing. **Liying Zhao:** Investigation, Data curation, Writing - original draft. **Dongxiao Wen:** Formal analysis, Conceptualization, Writing - review & editing. **Xiaolan Wang:** Investigation, Data curation. **Huaixia Yang:** Methodology, Supervision, Project administration. **Weisheng Feng:** Funding acquisition, Writing - review & editing. **Jinming Kong:** Funding acquisition, Project administration, Writing - review & editing.

Acknowledgements

This work was supported by four funds: The National Key Research and Development Project (The Major Project for Research of the Modernization of TCM): Key Technology Research for the Characteristic Chinese Medicine Industry Chain of Rehmannia glutinosa (2017YFC1702800); The Major Science and Technology Projects in Henan Province: Study on the key technology for quality control and the key characteristics of Rehmannia glutinosa, Dioscorea opposita Thunb and Achyranthes bidentata Blume from Henan Province (171100310500); The project of tackling of key scientific and technical problems in Henan Province (192102310033); National Natural Science Foundation of China (21575066).

References

[1] Y.Y. Sun, Q.X. Ren, B. Liu, Y. Qin, S. Zhao, Enzyme-free and sensitive electrochemical determination of the FLT3 gene based on a dual signal amplified strategy: controlled nanomaterial multilayers and a target-catalyzed hairpin assembly, Biosens. Bioelectron. 78 (2016) 7–13 https://doi.org/10.1016/j.bios.2015.11.014.
[2] L.D.S. Lapitan, Y.H. Xu, Y. Guo, D.J. Zhou, Combining magnetic nanoparticle capture and poly-enzyme nanobead amplification for ultrasensitive detection and discrimination of DNA single nucleotide polymorphisms, Nanoscale 11 (2019) 1195–1204 https://doi.org/10.1039/c8nr07641c.
[3] L.H. Tang, Y. Wang, J.H. Li, The graphene/nucleic acid nanobiointerface, Chem. Soc. Rev. 44 (2015) 6954–6980 https://doi.org/10.1039/c4cs00519h.
[4] R. Hansel-Hertsch, M. Di Antonio, S. Balasubramanian, DNA G-quadruplexes in the human genome: detection, functions and therapeutic potential, Nat. Rev. Mol. Cell Biol. 18 (2017) 279–284 https://doi.org/10.1038/nrm.2017.3.
[5] F.C. Loo, S.P. Ng, C.M.L. Wu, S.K. Kong, An aptasensor using DNA aptamer and white light common-path SPR spectral interferometry to detect cytochrome-c for anti-cancer drug screening, Sens. Actuators, B 198 (2014) 416–423 https://doi.org/10.1016/j.snb.2014.03.077.
[6] M.E. Kyriazi, D. Giust, A.H. El-Sagheer, P.M. Lackie, O.L. Muskens, T. Brown, A.G. Kanaras, Multiplexed mRNA sensing and combinatorial-targeted drug delivery using DNA-gold nanoparticle dimers, ACS Nano 12 (2018) 3333–3340 https://doi.org/10.1021/acsnano.7b08620.
[7] A. Araujo, W.W. Hall, Human T-lymphotropic virus type II and neurological disease, Ann. Neurol. 56 (2004) 10–19 https://doi.org/10.1002/ana.20126.
[8] V.S. Kalyanaraman, M.G. Sarngadharan, M. Robert-Guroff, I. Miyoshi, D. Golde, R.C. Gallo, A new subtype of human T- cell leukemia virus (HTLV-II) associated with a T-cell variant of hairy cell leukemia, Science 218 (1982) 571–573 https://doi.org/10.1126/science.6981847.
[9] L.J. Wang, M. Ren, L. Liang, C.Y. Zhang, Controllable fabrication of bio-bar codes for dendritically amplified sensing of human T-lymphotropic viruses, Chem. Sci. 9 (2018) 4942–4949 https://doi.org/10.1039/c8sc01641k.
[10] D. Cheng, Y.P. Zhang, D.X. Wen, Z.Z. Guo, H.X. Yang, Y.J. Liu, J.M. Kong, Hairpin probes based click polymerization for label-free electrochemical detection of human T-lymphotropic virus types II, Anal. Chim. Acta 1059 (2019) 86–93 https://doi.org/10.1016/j.aca.2019.01.027.
[11] D.D. Ho, T. Moudgil, M. Alam, Quantitation of human immunodeficiency virus type 1 in the blood of infected persons, N. Engl. J. Med. 321 (1989) 1621–1625 https://doi.org/10.1056/NEJM198912143212401.
[12] R. Chinnappan, R. Mohammed, A. Yaqinuddin, K. Abu-Salah, M. Zourob, Highly sensitive multiplex detection of microRNA by competitive DNA strand displacement fluorescence assay, Talanta 200 (2019) 487–493 https://doi.org/10.1016/j.talanta.2019. 03.061.
[13] X.M. Shi, G.C. Fan, X.Y. Tang, Q.M. Shen, J.J. Zhu, Ultrasensitive photoelectrochemical biosensor for the detection of HTLV-I DNA: a cascade signal amplification strategy integrating lambda-exonuclease aided target recycling with hybridization chain reaction and enzyme catalysis, Biosens. Bioelectron. 109 (2018) 190–196 https://doi.org/10.1016/j.bios.2018.03.023.
[14] N.N. Maslakci, F.D. Danas, A.U. Oksuz, QCM-DNA biosensor based on plasma modified PT/TiO_2 nanocomposites, J. Macromol. Sci., Pure Appl. Chem. 53 (2016) 311–316 https://doi.org/10.1080/10601325.2016.1151651.
[15] J.P. Li, S. Yang, W.Y. Zhou, C.H. Liu, Y.H. Jia, J. Zheng, Y.H. Li, J.S. Li, R.H. Yang, A gold nanocarrier and DNA-metalligation-based sensing ensemble for fluorescent assay of thiol-containing amino acids and peptides, Chem. Commun. 49 (2013) 7932–7934 https://doi.org/10.1039/c3cc44184a.
[16] H. Xu, S.X. Zhang, C.H. Ouyang, Z.M. Wang, D. Wu, Y.Y. Liu, Y.F. Jiang, Z.S. Wu, DNA nanostructures from palindromic rolling circle amplification for the fluorescent detection of cancer-related microRNAs, Talanta 192 (2019) 175–181 https://doi.org/10.1016/j.talanta.2018.07.090.
[17] S.L. Li, W.W. Qiu, X. Zhang, J.C. Ni, F. Gao, Q.X. Wang, A high-performance DNA biosensor based on the assembly of gold nanoparticles on the terminal of hairpin-structured probe DNA, Sens. Actuators, B 223 (2016) 861–867 https://doi.org/10.1016/j.snb.2015.09.121.
[18] T. Wang, Z. Zhang, Y.Y. Li, G.M. Xie, Amplified electrochemical detection of mecA gene in methicillin-resistant Staphylococcus aureus based on target recycling amplification and isothermal strand-displacement polymerization reaction, Sens. Actuators, B 22 (2015) 148–154 https://doi.org/10.1016/j.snb.2015.06.057.
[19] X.F. Zhang, R. Cheng, Z.L. Shi, Y. Jin, A PCR-free fluorescence strategy for detecting telomerase activity via double amplification strategy, Biosens. Bioelectron. 75 (2016) 101–107 https://doi.org/10.1016/j.bios.2015.08.013.

[20] C. Hong, A. Baek, S.S. Hah, W. Jung, D.E. Kim, Fluorometric detection of microRNA using isothermal gene amplification and graphene oxide, Anal. Chem. 88 (2016) 2999–3003 https://doi.org/10.1021/acs.analchem.6b00046.
[21] D. Li, S.P. Song, C.H. Fan, Target-responsive structural switching for nucleic acid-based sensors, Acc. Chem. Res. 43 (2010) 631–641 https://doi.org/10.1021/ar900245u.
[22] H.F. Dong, X.D. Meng, W.H. Dai, Y. Cao, H.T. Lu, S.F. Zhou, X.J. Zhang, Highly sensitive and selective microRNA detection based on DNA-bio-bar-code and enzyme-assisted strand cycle exponential signal amplification, Anal. Chem. 87 (2015) 4334–4340 https://doi.org/10.1021/acs.analchem.5b00029.
[23] J. Chao, Z.H. Li, J. Li, H.Z. Peng, S. Su, Q. Li, C.F. Zhu, X.L. Zuo, S.P. Song, L.H. Wang, L.H. Wang, Hybridization chain reaction amplification for highly sensitive fluorescence detection of DNA with dextran coated microarrays, Biosens. Bioelectron. 81 (2016) 92–96 https://doi.org/10.1016/j.bios.2016.01.093.
[24] Z.T. Allen, J.R. Sackey-Addo, M.P. Hopps, D. Tahseen, J.T. Anderson, T.A. Graf, C.B. Cooley, Fluorogenic atom transfer radical polymerization in aqueous media as a strategy for detection, Chem. Sci. 10 (2019) 1017–1022 https://doi.org/10.1039/c8sc03938k.
[25] G.R. Jones, A. Anastasaki, R. Whitfield, N. Engelis, E. Liarou, D.M. Haddleton, Copper-mediated reversible deactivation radical polymerization in aqueous media, Angew. Chem. Int. Ed. 57 (2018) 10468–10482 https://doi.org/10.1002/anie.201802091.
[26] U.C. Palmiero, M. Sponchioni, N. Manfredini, M. Maraldi, D. Moscatelli, Strategies to combine ROP with ATRP or RAFT polymerization for the synthesis of biodegradable polymeric nanoparticles for biomedical applications, Polym. Chem. 9 (2018) 4084–4099 https://doi.org/10.1039/c8py00649k.
[27] J. Su, X.W. He, L.X. Chen, Y.K. Zhang, A combination of "thiol - ene" click chemistry and surface initiated atom transfer radical polymerization: fabrication of boronic acid functionalized magnetic graphene oxide composite for enrichment of glycoproteins, Talanta 180 (2018) 54–60 https://doi.org/10.1016/j.talanta.2017.12.037.
[28] X.C. Pan, S. Lathwal, S. Mack, J.J. Yan, S.R. Das, K. Matyjaszewski, Automated synthesis of well-defined polymers and biohybrids by atom transfer radical polymerization using a DNA synthesizer, Angew. Chem. Int. Ed. 56 (2017) 2740–2743 https://doi.org/10.1002/anie.201611567.
[29] J.S. Wang, K. Matyjaszewski, Controlled/"Living" radical polymerization. atom transfer radical polymerization in the presence of transition-metal complexes, J. Am. Chem. Soc. 117 (1995) 5614–5615 https://doi.org/10.1021/ja00125a035.
[30] M. Kato, M. Kamigaito, M. Sawamoto, T. Higashimura, Polymerization of methyl methacrylate with the carbon tetrachloride/dichlorotris-(triphenylphosphine) ruthenium(II)/methylaluminum bis(2,6-di-tert-butylphenoxide) initiating system: possibility of living radical polymerization, Macromolecules 28 (1995) 1721–1723 https://doi.org/10.1021/ma00109a056.
[31] F. Seidi, H. Salimi, A.A. Shamsabadi, M. Shabanian, Synthesis of hybrid materials using graft copolymerization on non-cellulosic polysaccharides via homogenous ATRP, Prog. Polym. Sci. 76 (2018) 1–39 https://doi.org/10.1016/j.progpolymsci.2017.07.006.
[32] M.M. Lino, S. Simoes, A. Vilaca, H. Antunes, A. Zonari, L. Ferreira, Modulation of angiogenic activity by light-activatable miRNA-loaded nanocarriers, ACS Nano 12 (2018) 5207–5220 https://doi.org/10.1021/acsnano.7b07538.
[33] H.Y. Song, X.D. Zhou, J. Hobley, X.D. Su, Comparative study of random and oriented antibody immobilization as measured by dual polarization interferometry and surface plasmon resonance spectroscopy, Langmuir 28 (2012) 997–1004 https://doi.org/10.1021/la202734f.
[34] R. Martinez-Manez, F. Sancenon, Fluorogenic, chromogenic chemosensors and reagents for anions, Chem. Rev. 103 (2003) 4419–4476 https://doi.org/10.1021/cr010421e.
[35] S. Hansson, V. Trouillet, T. Tischer, A.S. Goldmann, A. Carlmark, C. Barner-Kowollik, E. Malmstrom, Grafting efficiency of synthetic polymers onto biomaterials: a comparative study of grafting-from versus grafting-to, Biomacromolecules 14 (2013) 64–74 https://doi.org/10.1021/bm3013132.
[36] P. Alonso-Cristobal, P. Vilela, A. El-Sagheer, E. Lopez-Cabarcos, T. Brown, O.L. Muskens, J. Rubio-Retama, A.G. Kanaras, Highly sensitive DNA sensor based on upconversion nanoparticles and graphene oxide, ACS Appl. Mater. Interfaces 7 (2015) 12422–12429 https://doi.org/10.1021/am507591u.
[37] L. Ma, N.N. Sun, J.Y. Zhang, C.H. Tu, X.Q. Cao, D.M. Duan, A.P. Diao, S.L. Man, Polyethylenimine-coated Fe_3O_4 nanoparticles effectively quench fluorescent DNA, which can be developed as a novel platform for protein detection, Nanoscale 9 (2017) 17699–17703 https://doi.org/10.1039/c7nr07085c.
[38] S. Lukman, K.M.M. Aung, M.G.L. Lim, S.Z. Hong, S.K. Tan, E. Cheung, X.D. Su, Hybrid assembly of DNA-coated gold nanoparticles with water soluble conjugated polymers for studying protein-DNA interaction and ligand inhibition, RSC Adv. 4 (2014) 8883–8893 https://doi.org/10.1039/C3RA46752J.
[39] P. Leophairatana, S. Samanta, C.C. De Silva, J.T. Koberstein, Preventing alkyne-alkyne (i.e., glaser) coupling associated with the ATRP synthesis of alkyne-functional polymers/macromonomers and for alkynes under click (i.e., CuAAC) reaction conditions, J. Am. Chem. Soc. 139 (2017) 3756–3766 https://doi.org/10.1021/jacs.6b12525.
[40] L.A. Yuan, Y.F. Wu, H.Y. Shi, S.Q. Liu, Surface-initiated atom-transfer radical polymerization of 4-acetoxystyrene for immunosensing, Chem. Eur J. 17 (2011) 976–983 https://doi.org/10.1002/chem.201001271.
[41] W.M. Zheng, L. He, Particle stability in polymer-assisted reverse colorimetric DNA assays, Anal. Bioanal. Chem. 393 (2009) 1305–1313 https://doi.org/10.1007/s00216-008-2536-4.
[42] Q. Hu, J.M. Kong, Y.J. Li, X.J. Zhang, A signal-on electrochemical DNA biosensor based on potential-assisted Cu(I)-catalyzed azide-alkyne cycloaddition mediated labeling of hairpin-like oligonucleotide with electroactive probe, Talanta 147 (2016) 516–522 https://doi.org/10.1016/j.talanta.2015.10.039.
[43] M. Chen, Y.Y. Wang, H.L. Su, L. Mao, X.N. Jiang, T. Zhang, X.Z. Dai, Three-dimensional electrochemical DNA biosensor based on 3D graphene-Ag nanoparticles for sensitive detection of CYFRA21-1 in non-small cell lung cancer, Sens. Actuators, B 255 (2018) 2910–2918 https://doi.org/10.1016/j.snb.2017.09.111.
[44] Q. Hu, Q.W. Wang, J.M. Kong, L.Z. Li, X.J. Zhang, Electrochemically mediated in situ growth of electroactive polymers for highly sensitive detection of double-stranded DNA without sequence-preference, Biosens. Bioelectron. 101 (2018) 1–6 https://doi.org/10.1016/j.bios.2017.09.045.
[45] J.H. Huang, J.Q. Wu, Z.G. Li, Molecular beacon-based enzyme-free strategy for amplified DNA detection, Biosens. Bioelectron. 79 (2016) 758–762 https://doi.org/10.1016/j.bios.2016.01.014.
[46] S.F. Liu, C.B. Cheng, T. Liu, L. Wang, H.W. Gong, F. Li, Highly sensitive fluorescence detection of target DNA by coupling exonuclease-assisted cascade target recycling and DNAzyme amplification, Biosens. Bioelectron. 63 (2015) 99–104 https://doi.org/10.1016/j.bios.2014.07.023.